Sensors and Actuators: A. Physical xxx (xxxx) xxx

Contents lists available at ScienceDirect

Sensors and Actuators: A. Physical

journal homepage: www.elsevier.com/locate/sna

Tilting micromirror platform based on liquid dielectrophoresis

Iman Frozanpoor[a,*], Michael Cooke[a], Diana Alvarez-Ruiz[b], Vibin Ambukan[c], Andrew Gallant[a], Claudio Balocco[a]

[a] Department of Engineering, Durham University, South Rd, Durham DH1 3LE, UK
[b] Department of Physics, Durham University, Lower Mountjoy, South Rd, Durham DH1 3LE, UK
[c] Jaguar Land Rover Limited, National Automotive Innovation Centre, Coventry CV4 7AL, UK

ARTICLE INFO

Article history:
Received 15 July 2021
Received in revised form 14 September 2021
Accepted 12 October 2021
Available online xxxx

Keywords:
Liquid dielectrophoresis
Micromirror platform
Beam steering
Droplet actuation
Hydrophobicity

ABSTRACT

This study presents an electrically actuated tilting micro platform based on liquid dielectrophoresis with three axes movement using three droplets situated 120° apart from each other. The interdigitated electrodes produce a non-uniform electric field that generates a body force. The dielectrophoretic mechanism is responsive within at least 30 ms, and it eliminates the solid-solid contact. The tilting platform enabled an angular coverage up to 0.9° (±0.02°), with a maximum displacement of 120 µm. The tilting micromirror platform has beam steering characteristics suitable for various optical applications. The actuating platform sensor is a cost-effective and simple alternative method to study liquid dielectrophoresis without measuring the droplet contact angle. Furthermore, the unique configuration without any solid-solid contact offers a potential improvement for applications in optics, actuators, and other conventional microelectromechanical systems.

1. Introduction

Electrically controlled tilting mirrors play an important role in several modern technologies. They are typically found in many related research fields, including microscopy, micromachining, micropositioning, and lithography [1,2]. The application of a micromirror can be found in optical devices [3,4], tuneable lasers [5], 3D scanning using light detection and ranging (LIDAR) [6], and imaging technologies [7]. Typically, they are compact and lightweight, presenting a ubiquitous solution for beam steering [8]. For example, the conventional microelectromechanical systems (MEMS) micromirror consists of a reflective plate attached to a support structure with springs allowing movement in a tip-tilt or piston mode [9]. The technology has been steadily growing, and the recent developments are focusing on affordability, high-speed motion, and a wide field of view [10].

There are several reported actuation mechanisms for different applications. For example, electromagnetic actuators [11], pneumatic actuators [12], electrothermal actuators [13], electrostatic actuators [14,15], and piezoelectric actuators [16]. Typically, the electrostatic systems can generate a mechanical motion by a change of stationary electric field in materials. They typically exhibit unique characteristics, such as a fast response, wide scanning angle, and low power consumption. Furthermore, the size of the electrostatic platforms are between 0.5 mm and 10 mm, with a wide operating voltage between 5 V and 250 V, and a large range of scanning angle from 0.6° to 146° [10].

This paper describes an actuation system based on the electrostatic forces generated by the interdigitated electrodes (IDE's). Liquid dielectrophoresis (L-DEP) is a bulk electrostatic force generated near the droplet solid-liquid interface when applying a non-uniform electric field [17]. The electrostatic actuation is suitable for various liquids, such as water, oil-based solutions, liquid crystals, solvents, and organic compounds [18].

The dielectrophoretic force depends on the liquid permittivity, in addition to the strength and penetration depth of the non-uniform electric field [19]. The electrostatic behaviour is also frequency-dependent [20]. For example, the ionic conductivity above a critical signal frequency (typically in the kilohertz region) is negligible in deionised (DI) water, and thus the liquid behaves as a dielectric body [21].

The typical L-DEP device consists of an electrode pad (i.e., IDE's), covered by an insulating layer with a hydrophobic coating [22]. Several other electrode configurations have also demonstrated droplet manipulation using L-DEP [23–25]. They typically consist of an array of larger pads situated in planar or sandwich configurations [2]. Furthermore, recent developments demonstrated that a

* Corresponding author.
E-mail address: iman.frozanpoor@durham.ac.uk (I. Frozanpoor).

https://doi.org/10.1016/j.sna.2021.113177
0924-4247/

Please cite this article as: I. Frozanpoor, M. Cooke, D. Alvarez-Ruiz et al., Tilting micromirror platform based on liquid dielectrophoresis, Sensors and Actuators: A. Physical, https://doi.org/10.1016/j.sna.2021.113177

continuous droplet actuation is possible using variable interdigitated electrodes (VIDE's) [26].

The bulk L-DEP force rapidly rises with an increase of the applied voltage up to the voltage breakdown limit of the insulating layer [27]. However, L-DEP can overcome the contact angle saturation limitation of electrowetting to achieve a complete film formation using several hundred volts [28].

There are several methods employed to study the L-DEP phenomenon. The most common method is measuring the change in contact angle of a droplet upon applying a non-uniform electric field [28]. The manipulation of the contact line has been characterised by the electrostatic body force equations and interface localised L-DEP using Young's equation [17]. Furthermore, liquid manipulation has also been characterised using Pellat's experiment of rising liquid height [20], and the droplet actuation speed using a high-speed camera [29].

L-DEP is a promising method for optical switches and displays, liquid iris, optical beam steering, and liquid lenses [30–33]. However, we aim to explore an alternative optical application for this technology to develop a tilting mirror platform with beam steering for applications in actuators, micro-optics, and other MEMS devices. The micromirror is also suitable for studying L-DEP without measuring the droplet contact angle.

2. Materials and methods

2.1. Design and fabrication

This paper reports on a tilting mirror supported by three DI water droplets whose height is actuated using the L-DEP mechanism. Fig. 1(a) shows the structure of the device that generated the L-DEP force that consists of four separate layers (in sequenced order: substrate, electrodes, insulating layer, and a functionalised hydrophobic layer). The substrate was borosilicate glass. Initially, 70 nm of aluminium was deposited by E-beam evaporation on the glass substrate, and IDE's with a gap distance of 20 µm were fabricated using standard photolithography. Fig. 1(b) shows the top view microscopic image of the IDE's. The IDE's design is typical in dielectrowetting studies. However, the electrode gap distance is usually larger (in order of hundreds of micrometres), and the operating voltages are in excess of several hundred volts [28]. The insulating layer was aluminium oxide (400 nm), deposited using atomic layer deposition (ALD). Aluminium oxide was chosen because of its insulating properties while also providing good chemical and mechanical protection.

Aluminium oxide was functionalised with a self-assembled monolayer (SAM), octadecyltrichlorosilane (OTS), to improve the surface hydrophobicity (110° ± 4°) [34]. Moreover, the use of SAM OTS hydrophobic coating in dielectrowetting and electrowetting studies has already been reported [22,26,35]. Solution of hexane/OTS (1 part of OTS in 500 parts of hexane by volume) was prepared and sonicated for 10 min for better uniformity. The samples were immersed inside the solution for 7 h without agitation. The samples were immediately washed with hexane and dried using filtered nitrogen gas. Lastly, the samples were baked for 10 min at 95 °C to complete the OTS polymerisation process. Furthermore, Fig. 1(c) shows the side view image of the micromirror platform during operation.

Also, Fig. 1(a) shows the reflective cover plate with four separate layers. The base substrate was mica (15 mm × 15 mm), with a nominal thickness of 0.1 mm. Firstly, 100 nm of aluminium was deposited using E-beam evaporation on the mica substrate to act as a reflective surface. The droplet compression effect was minimised using a superhydrophobic coating, as the untreated mica surface was hydrophilic. Fig. 2(a) shows the SAM OTS hydrophobic coating on a fabric

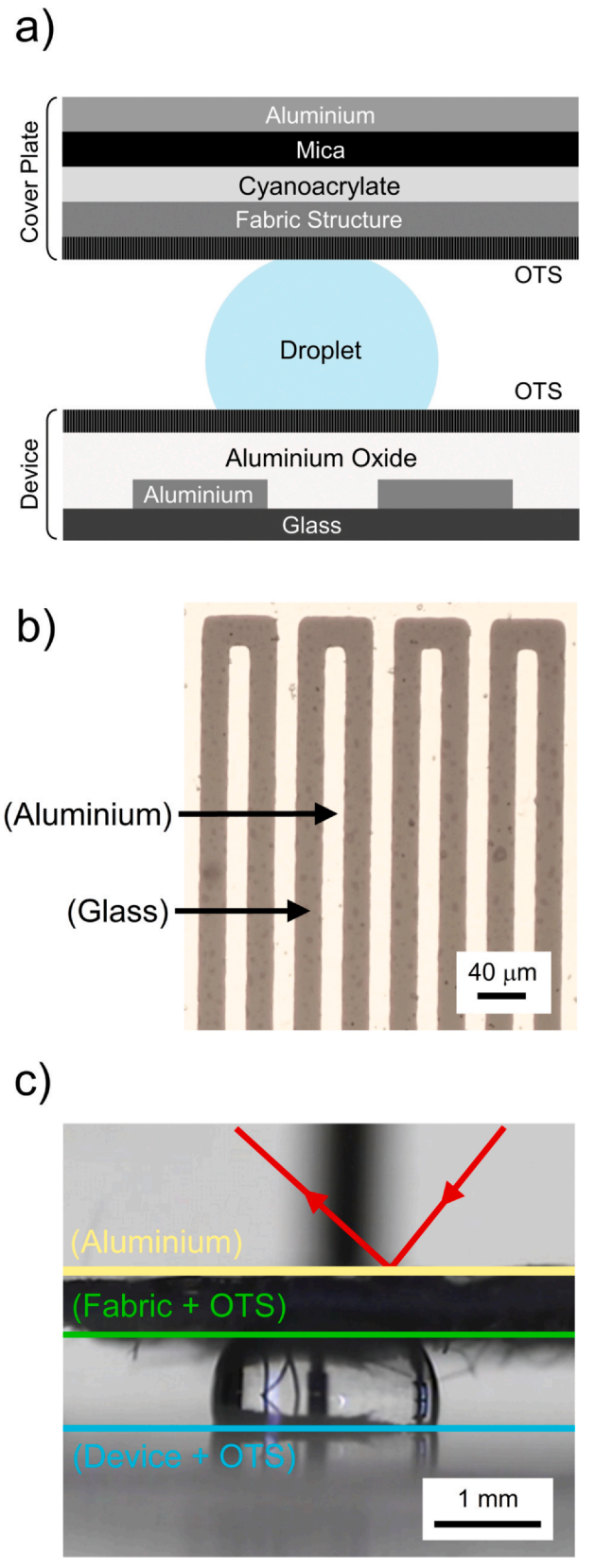

Fig. 1. (a) Fabrication structure of a device with a lightweight cover plate. (b) The top view image of the IDE's with a gap distance of 20 µm. Note that the impurities on the surface are OTS residuals polymerised after the hard-bake process. The higher surface roughness improves hydrophobic properties. (c) The side view image of a device during operation. The testing liquid was DI water, and the arrows show the laser beam bouncing off the reflective surface.

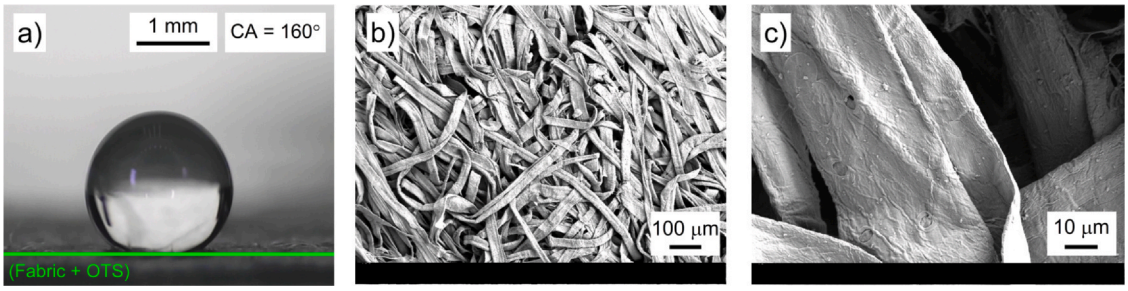

Fig. 2. (a) The side-view image showing a superhydrophobic surface with a contact angle of 160°. (b) SEM image with a magnification of (100 X) showing the micro-scale entangled fabric structures. The irregular and large surface features enable a lightweight modification with a higher contact angle. (c) SEM image with a magnification (1000 X) showing a typical fibre with SAM OTS surface treatment.

structure (cleanroom wipes), leading to a contact angle of 160°. A similar surface treatment was demonstrated for developing humidity-resistant fabric coating using SAM OTS for wearable triboelectric energy harvesting [36]. However, a higher contact was observed in our study because of the unique surface morphology of the cleanroom wipes. Fig. 2(b, c) show scanning electron microscope (SEM) images with different magnification at 5.0 kV using Carl Zeiss Sigma VP 300 FEG-SEM. The samples were sputter coated with 20 nm of gold prior to SEM observations.

The images verified that superhydrophobicity was obtained via these micro-scale fabric structures treated with SAM OTS. Figure (S1) shows SEM images comparing surface features before and after SAM OTS treatment. The surface roughness (fibres networking on the surface) had a considerable influence on the droplet contact angle, producing a superhydrophobic surface [37]. The material consisted of 45% polyester and 55% cellulose, with an entangled fabric structure (micro-scale) and a basis weight of 67 g/m^2. The droplet rests on a patchwork of air and solid interface, and the low surface energy prevents the liquid interface from penetrating within the roughness, leading to a high contact angle. The testing liquid was DI water; nevertheless, other liquids are similarly compatible, including other organic compounds such as propylene carbonate.

2.2. Experimental setup

Fig. 3(a) shows the general overview of the tilting micromirror platform. The working function of the device was based on three IDE's (4 mm × 4 mm), situated 120° apart from each other. Please refer to the supplementary material for more details about the set up parameters. Initially, the laser beam was focused on the centre of the mirror plate at an angle of 45°. The laser beam was reflected off to an observation panel, where a recording camera monitored the beam movement. Fig. 3(b) shows a typical test results using 60 V. The upper edge of the beam was used as the reference point to measure the beam movement. The laser beam position was accurate with a precision of up to ± 500 µm, and the movement of the laser beam was several centimetres, making it easy to detect using a recording camera. The alternating current (AC) voltages denote root-mean-square, and direct current (DC) voltages were avoided because of lower electric field penetration.

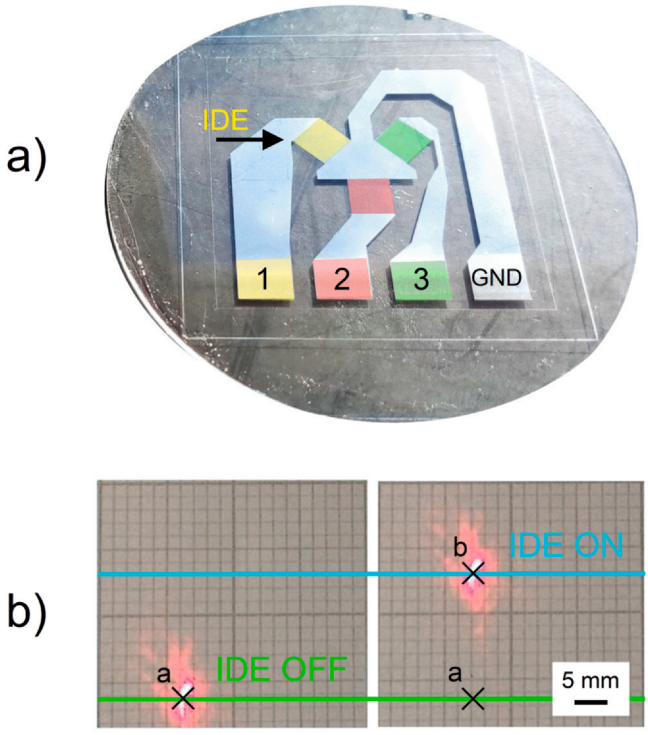

Fig. 3. (a) The top view image of the device showing the three control electrodes; each pad is 120° apart, with three control electrodes and a common ground (GND). (b) The testing results show the laser movement (a-OFF and b-ON). The spacing between the square grid patterns is 2 mm.

3. Results and discussion

3.1. Contact angle measurements

Fig. 4 confirms the fundamental nonlinear relation between electrowetting and L-DEP, in which the cosine of Young's contact angle (θ_y) is proportional to the voltage squared. Testing results were measured using a contact angle goniometer, and they show that higher voltages generate a stronger electric field and, thus, nonlinearly increase the contact angle [38]. The operating voltage in other L-DEP studies was over 250 V, with a thick insulating and hydrophobic layer (a few micrometres) that limited the L-DEP effect at lower voltages [21,28]. The applied voltage in our study was minimised by reducing the IDE's gap distance to 20 µm, in addition to reducing the insulating and hydrophobic thickness to approximately 400 nm to maximise the penetration distance of the electric field.

3.2. Optical measurements using the micromirror

Conventional beam steering designs, for example piezoelectric actuators, are based on solid parts whose structures are rigid, and therefore, limited by the stiction effect of moving parts [39]. Controlling the contact angle of droplets situated under a mirror plate provided a three-axis tilt mechanism for beam steering. The beam's position can be precisely controlled via regulating the signal frequency or the applied voltage to individual electrode pads.

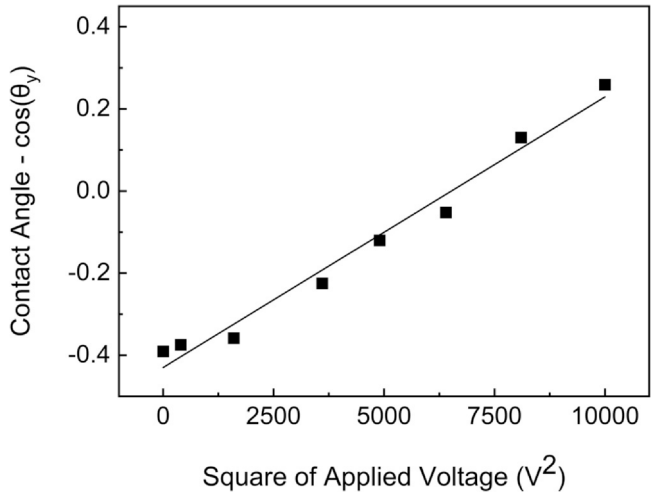

Fig. 4. The relationship between cosine of contact angle and square of applied voltage. The measurements were made using a contact angle goniometer, and they highlight the device performance at different voltages. Note that θ_y is the static Young's contact angle.

Furthermore, it is possible to generate geometries (such as triangles or circles) by switching a sequence of IDE's.

Changes in the droplet contact angle result in the displacement of the mirror plate. In addition to the MEMS optical applications, the platform is also suitable for studying the L-DEP actuation mechanism. This is an alternative method to study the L-DEP phenomenon. Other conventional methods include contact angle measurements and the rise of liquid in the parallel plates [22,40]. The main advantages of using our method is that it is cost effective and easy to set up, since it does not require a contact angle goniometer. Furthermore, it is capable of collecting accurate measurements requiring minimal video processing for dynamic actuations.

The important testing parameters are the deflection distance δ, which is the mirror plate's vertical movement, and the beam's angle of deflection, θ. Fig. 5(a) shows the angle of deflection and deflection distance of the mirror plate versus the drive voltage (up to 100 V) for a fixed signal frequency of 30 kHz. These results confirm that the performance increases nonlinearly with the applied voltage. The dielectrophoretic force is dependent on the strength of the electric field, and thus a higher applied voltage produces larger forces [19]. Fig. 5(b), presents the frequency-dependent experimental results. The applied voltage was fixed at 60 V for a frequency sweep between 100 Hz and 2 MHz. Furthermore, the testing results showed that the optimum performance was between 20 kHz and 30 kHz. The thickness of the dielectric layer can change the critical frequency. Previous investigations demonstrated that the critical frequency could change from 60 kHz to 10 kHz when the insulating thickness reduces from 10 µm to 2 µm, respectively [41]. The L-DEP force is strongly dependent on the signal frequency, and the effect is dominant when the applied frequency is more than 10 kHz and significantly diminishes after 500 kHz.

Fig. 6(a) shows the dynamic performance for two modulated signal (square wave) frequencies (0.5 Hz and 10 Hz), with a fixed sine-wave carrier signal at 20 kHz. The droplet spreading behaviour on IDE's exhibit a small degree of contact angle hysteresis when swapping between advancing and receding contact angles [42]. This will translate into inaccuracies in the position of the mirror. However, this effect is only detected in the first activation cycle (OFF-ON-OFF), as depicted in Fig. 6(a) with dotted lines. On the other hand, the small hysteresis translates into ± 0.01° of angular change, and therefore, it can be neglected in applications where there is a large

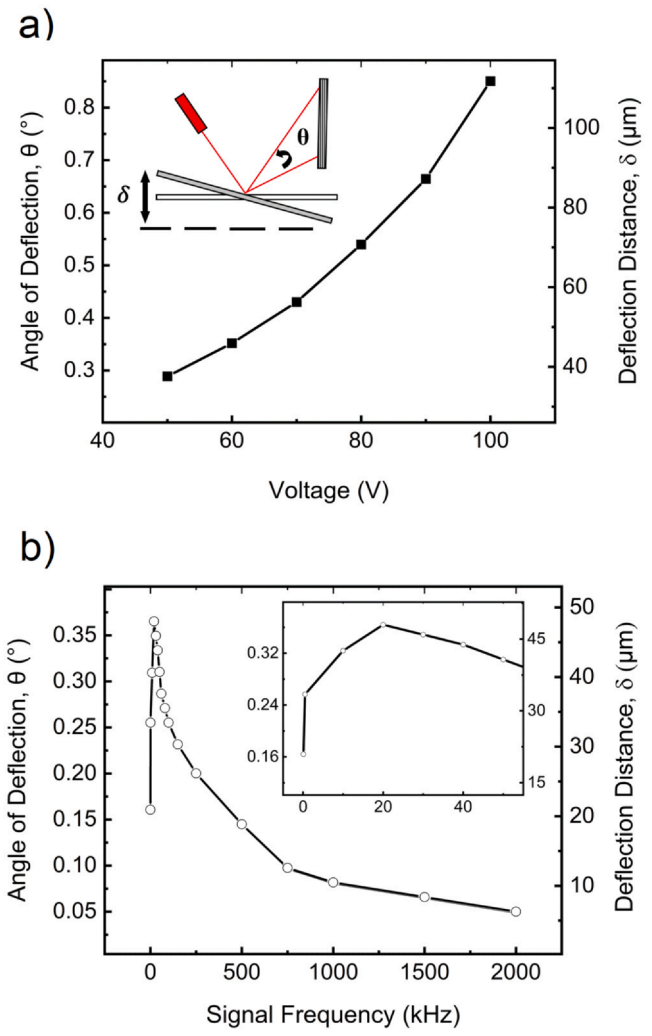

Fig. 5. The experimental measurements using the micromirror platform. (a) The voltage-dependent testing results at a fixed signal frequency of 30 kHz. The subfigure shows the two important testing parameters: the optical angle of deflections and the deflection distance of the mirror plate. (b) The experimental results showing the frequency-dependent behaviour (100 Hz to 2 MHz) at 60 V. The subfigure shows the results up to 50 kHz.

variation in the angle of deflection. Alternatively, regulating both the signal frequency and the applied voltage may reduce the hysteresis when swapping from advancing to receding angles in the initial switching cycle, at the expense of a more complex control system.

Fig. 6(b) shows the range of optical angle of deflection (between ON and OFF state) with a fixed signal frequency of 20 kHz at different modulated signal frequencies (0.5–500 Hz). The droplet spreading time was 30 ms and 170 ms when the device was turned ON and OFF, respectively. Consequently, a modulated signal with a frequency exceeding 2 Hz surpasses the liquid hydrodynamic response. Therefore, factors influencing the liquid hydrodynamic response should be considered depending on the application. Several examples are droplet size [43], liquid viscosity [44], temperature [45], and the balance between interfacial and electrostatic energies [46]. Moreover, the spreading speed was 33.3 mm s^{-1} and 5.8 mm s^{-1} when the device was turned ON and OFF, respectively. This is also similar to the measured experimental data using a contact angle goniometer, as reported elsewhere [47]. The dynamic experimental results using different modulated signal frequencies demonstrate a

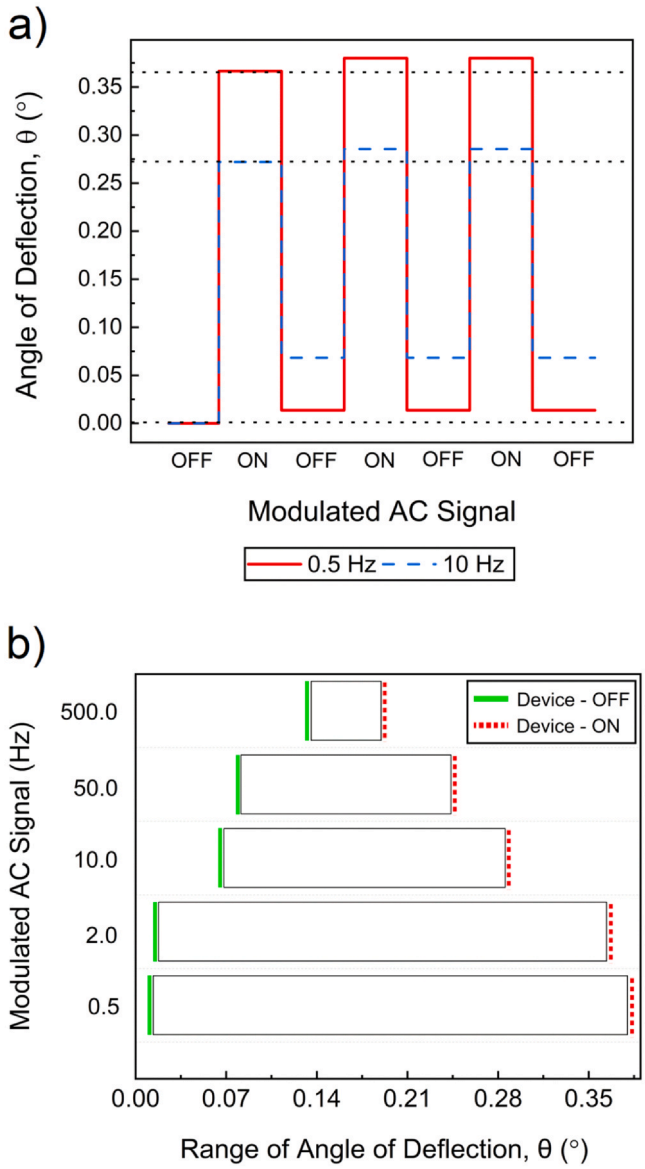

Fig. 6. The experimental measurements using the micromirror platform. (a) The testing results showing the modulation of the angle of deflection. The dotted lines highlight the range in the angle of deflection when swapping from the advancing to receding contact angles. (b) The range of angle of deflection with a fixed signal frequency of 20 kHz at different modulated signal frequencies (0.5–500 Hz). Note that the left (red) and right (green) side of each bar shows the modulated value of θ when the device switches from an OFF-state into an ON-state.

reliable testing method for studying L-DEP, comparable to analysis using contact angle measurements.

A vertical translation and angular manipulation stage was demonstrated using electrowetting-on-dielectric (EWOD) in a previous study [48]. There are several key differences between an actuating platform using L-DEP and EWOD. Predominantly, the electrode configuration using L-DEP is planar, meaning that the signal and ground electrodes are located in the same plane. Thus, translating to simpler modifications such as using a filter paper to produce a superhydrophobic surface. Secondly, the L-DEP mechanism is compatible with dielectric liquids. Therefore, the testing droplets can be oil-based solutions, liquid crystals, and organic compounds with a lower evaporation rate. Additionally, lower operating voltages are achieved by scaling down the electrode dimensions to the micron scale, and also, L-DEP can overcome the contact angle saturation limitation of electrowetting, and therefore further refinement is feasible at lower voltages.

4. Conclusions

An electrostatic actuator micromirror based on the L-DEP mechanism was presented in this paper. The platform demonstrated beam steering capabilities for optical applications. Furthermore, the platform was also presented as an alternative method to study the L-DEP mechanism without measuring the droplet contact angle. The tilting platform enabled an angular coverage up to 0.9° (±0.02°), with a maximum displacement of 120 µm. Note that a superhydrophobic coating on both surfaces can readily improve the device performance because of higher changes in the spatial distance between the two surfaces, and thus further refinement is feasible.

Furthermore, the operating voltage was lowered (to less than 100 V), using electrodes with a 20 µm gap distance and an insulating layer with a thickness of 400 nm. This was significantly lower than other L-DEP studies using several hundred volts. Additionally, operating the tilting micro platform without solid-solid contact overcomes the limitations of the stiction effect for moving parts and other tribology concerns. The developments presented in this paper can assist researchers in designing novel actuating systems based on the L-DEP principle. A notable configuration is an array of micromirrors, opening new avenues for developing digital micromirror devices, MEMS scanning micromirrors, and optical switches in next-generation sensor networks.

Author statement

We the undersigned declare that this manuscript is original, has not been published before and is not currently being considered for publication elsewhere. We confirm that the manuscript has been read and approved by all named authors and that there are no other persons who satisfied the criteria for authorship but are not listed. We further confirm that the order of authors listed in the manuscript has been approved by all of us. We understand that the Corresponding Author is the sole contact for the Editorial process. He is responsible for communicating with the other authors about progress, submissions of revisions and final approval document.

Supplementary material

See supplementary material for the calculations of the deflection distance and angle of deflections. There are also SEM images comparing surfaces treated with and without SAM OTS. Movie (S1) shows the experimental method.

Supplementary material related to this article can be found online at doi:10.1016/j.sna.2021.113177.

Declaration of Competing Interest

The authors declare that they have no known competing financial interests or personal relationships that could have appeared to influence the work reported in this paper.

Acknowledgments

We are thankful for the financial support provided by Jaguar Land Rover and the Engineering and Physical Sciences Research Council

(EPSRC), United Kingdom, through the Industrial Case Award EP/P510476/1.

Appendix A. Supporting information

Supplementary data associated with this article can be found in the online version at doi:10.1016/j.sna.2021.113177.

References

[1] S.T.S. Holmström, U. Baran, H. Urey, MEMS laser scanners: a review, J. Microelectromech. Syst. 23 (2) (2014) 259–275.
[2] P. Teng, D. Tian, H. Fu, S. Wang, Recent progress of electrowetting for droplet manipulation: from wetting to superwetting systems, Mater. Chem. Front. 4 (1) (2020) 140–154.
[3] C.W. Oh, Z. Cao, E. Tangdiongga, T. Koonen, Free-space transmission with passive 2D beam steering for multi-gigabit-per-second per-beam indoor optical wireless networks, Opt. Express 24 (17) (2016) 19211–19227.
[4] C. Pollock, J. Morrison, M. Imboden, T.D.C. Little, D.J. Bishop, Beam shaping with tip-tilt varifocal mirror for indoor optical wireless communication, Opt. Express 25 (17) (2017) 20274–20285.
[5] A.Q. Liu, X.M. Zhang, A review of MEMS external-cavity tunable lasers, J. Micromech. Microeng. 17 (1) (2006) R1–R13.
[6] D. Wang, C. Watkins, H. Xie, MEMS mirrors for lidar: a review, Micromechines 11 (5) (2020) 456.
[7] Z. Qiu, W. Piyawattanametha, MEMS-based medical endomicroscopes, IEEE J. Sel. Top. Quantum Electron. 21 (4) (2015) 376–391.
[8] D. Sadhukhan, G.P. Singh, Study of electrostatic actuated MEMS biaxial scanning micro-mirror with comb structure, AIP Conf. Proc. 2269 (1) (2020) 030019.
[9] J. Morrison, M. Imboden, T.D.C. Little, D.J. Bishop, Electrothermally actuated tip-tilt-piston micromirror with integrated varifocal capability, Opt. Express 23 (7) (2015) 9555–9566.
[10] E. Pengwang, K. Rabenorosoa, M. Rakotondrabe, N. Andreff, Scanning micro-mirror platform based on MEMS technology for medical application, Micromachines 7 (2) (2016).
[11] J.J. Bernstein, W.P. Taylor, J.D. Brazzle, C.J. Corcoran, G. Kirkos, J.E. Odhner, A. Pareek, M. Waelti, M. Zai, Electromagnetically actuated mirror arrays for use in 3-D optical switching applications, J. Microelectromech. Syst. 13 (3) (2004) 526–535.
[12] A. Werber, H. Zappe, Tunable, membrane-based, pneumatic micro-mirrors, J. Opt. A: Pure Appl. Opt. 8 (7) (2006) S313–S317.
[13] S. Wang, Y. Hao, S. Liu, The design and analysis of a MEMS electrothermal actuator, J. Semicond. 36 (4) (2015) 044012.
[14] Y. Cao, P. Wang, J. Li, H. Xie, Temperature stability study of resonant angular scanning micromirrors with electrostatic comb-drive actuators, Sens. Actuators A 318 (2021) 112525.
[15] L.Y. Lin, E.G. Keeler, Progress of MEMS scanning micromirrors for optical bio-imaging, Micromachines 6 (11) (2015) 1675–1689.
[16] F. Lemke, P.M. Weber, K. Philipp, J.W. Czarske, N. Koukourakis, U. Wallrabe, M.C. Wapler, Piezo-actuated adaptive prisms for continuously adjustable bi-axial scanning, Smart Mater. Struct. 29 (9) (2020) 095004.
[17] A.M.J. Edwards, C.V. Brown, M.I. Newton, G. McHale, Dielectrowetting: the past, present and future, Curr. Opin. Colloid Interface Sci. 36 (2018) 28–36.
[18] J. Li, Y. Wang, H. Chen, J. Wan, Electrowetting-on-dielectrics for manipulation of oil drops and gas bubbles in aqueous-shell compound drops, Lab Chip 14 (22) (2014) 4334–4337.
[19] P.M. Young, K. Mohseni, Calculation of DEP and EWOD forces for application in digital microfluidics, J. Fluids Eng. 130 (8) (2008).
[20] T.B. Jones, K.L. Wang, D.J. Yao, Frequency-dependent electromechanics of aqueous liquids: electrowetting and dielectrophoresis, Langmuir 20 (7) (2004) 2813–2818.
[21] H. Geng, J. Feng, L.M. Stabryla, S.K. Cho, Dielectrowetting manipulation for digital microfluidics: creating, transporting, splitting, and merging of droplets, Lab Chip 17 (6) (2017) 1060–1068.
[22] I. Frozanpoor, M. Cooke, Z. Racz, I. Bossons, V. Ambukan, D. Wood, A. Gallant, C. Balocco, Programmable droplet actuating platform using liquid dielectrophoresis, J. Micromech. Microeng. 31 (5) (2021) 055014.
[23] H. Geng, S.K. Cho, Antifouling digital microfluidics using lubricant infused porous film, Lab Chip 19 (13) (2019) 2275–2283.
[24] J. Kedzierski, E. Holihan, Linear and rotational microhydraulic actuators driven by electrowetting, Sci. Robot 3 (22) (2018) eaat5643.
[25] R. Prakash, K.V.I.S. Kaler, Liquid dielectrophoresis dispensing of vesicles for on-chip nucleic acid isolation and detection, Colloids Surf., A Physicochem. Eng. Asp. 432 (2013) 42–49.
[26] I. Frozanpoor, M.D. Cooke, V. Ambukan, A.J. Gallant, C. Balocco, Continuous droplet-actuating platforms via an electric field gradient: electrowetting and liquid dielectrophoresis, Langmuir 37 (21) (2021) 6414–6422.
[27] C. Brown, W. Al-Shabib, G. Wells, G. McHale, M. Newton, Amplitude scaling of a static wrinkle at an oil-air interface created by dielectrophoresis forces, Appl. Phys. Lett. 97 (24) (2010) 242904.
[28] Z. Brabcova, G. McHale, G.G. Wells, C.V. Brown, M.I. Newton, Electric field induced reversible spreading of droplets into films on lubricant impregnated surfaces, Appl. Phys. Lett. 110 (12) (2017) 121603.
[29] A.M.J. Edwards, R. Ledesma-Aguilar, M.I. Newton, C.V. Brown, G. McHale, Not spreading in reverse: the dewetting of a liquid film into a single drop, Sci. Adv. 2 (9) (2016) e1600183.
[30] S. Xu, H. Ren, S.-T. Wu, Dielectrophoretically tunable optofluidic devices, J. Phys. D Appl. Phys. 46 (48) (2013) 483001.
[31] M. Oliva-Ramírez, S.-L. Wang, V. Rico-Gavira, C. López-Santos, S.-K. Fan, A.R. González-Elipe, Optofluidic liquid sensing on electromicrofluidic devices, Mater. Res. Express 7 (3) (2020) 036407.
[32] J. Wang, H. Wang, X. Li, Y. Zi, Self-powered electrowetting optical switch driven by a triboelectric nanogenerator for wireless sensing, Nano Energy 66 (2019) 104140.
[33] W. Cheng, J. Liu, Z. Zheng, X. He, B. Zheng, H. Zhang, H. Cui, X. Zheng, T. Zheng, B.E. Gnade, J. Cheng, Adaptive optical beam steering and tuning system based on electrowetting driven fluidic rotor, Commun. Phys. 3 (1) (2020) 25.
[34] J. Jin, L. Wang, Z. Zheng, J. Zhang, X. Hu, J.R. Lu, D. Etor, C. Pearson, A. Song, D. Wood, A.J. Gallant, C. Balocco, Metal-insulator-metal diodes based on alkyl-trichlorosilane self-assembled monolayers, AIP Adv. 9 (6) (2019) 065017.
[35] V. Kumar, N. Maheshwari, N.N. Sharma, Self assembled monolayer modified SU8 surface for electrowetting application, Macromol. Symp. 357 (1) (2015) 18–22.
[36] M.-O. Kim, S. Pyo, G. Song, W. Kim, Y. Oh, C. Park, C. Park, J. Kim, Humidity-resistant, fabric-based, wearable triboelectric energy harvester by treatment of hydrophobic self-assembled monolayers, Adv. Mater. Technol. 3 (7) (2018) 1800048.
[37] S. Parvate, P. Dixit, S. Chattopadhyay, Superhydrophobic surfaces: insights from theory and experiment, J. Phys. Chem. B 124 (8) (2020) 1323–1360.
[38] J. Barman, W. Shao, B. Tang, D. Yuan, J. Groenewold, G. Zhou, Wettability manipulation by interface-localized liquid dielectrophoresis: fundamentals and applications, Micromachines 10 (5) (2019) 329.
[39] M. Rezaei, J. Lueke, D. Raboud, W. Moussa, Challenges in fabrication and testing of piezoelectric MEMS with a particular focus on energy harvesters, Microsyst. Technol. 19 (8) (2013) 1195–1219.
[40] T.B. Jones, Liquid dielectrophoresis on the microscale, J. Electrost. 51–52 (2001) 290–299.
[41] T.B. Jones, On the relationship of dielectrophoresis and electrowetting, Langmuir 18 (11) (2002) 4437–4443.
[42] G. McHale, C.V. Brown, M.I. Newton, G.G. Wells, N. Sampara, Dielectrowetting driven spreading of droplets, Phys. Rev. Lett. 107 (18) (2011) 186101.
[43] Q. Vo, H. Su, T. Tran, Universal transient dynamics of electrowetting droplets, Sci. Rep. 8 (1) (2018) 836.
[44] X. Ren, S. Wei, X. Qu, F. Liu, Electrohydrodynamic analysis of electrowetting-on-dielectric (EWOD)-Induced transport of a microdroplet based on the lattice Boltzmann method, AIP Adv. 9 (5) (2019) 055021.
[45] P. García-Sánchez, A. Ramos, F. Mugele, Electrothermally driven flows in ac electrowetting, Phys. Rev. E 81 (1) (2010) 015303.
[46] A. Klingner, S. Herminghaus, F. Mugele, Self-excited oscillatory dynamics of capillary bridges in electric fields, Appl. Phys. Lett. 82 (23) (2003) 4187–4189.
[47] A.M.J. Edwards, R. Ledesma-Aguilar, M.I. Newton, C.V. Brown, G. McHale, Electrostatic control of dewetting dynamics, Appl. Phys. Lett. 116 (25) (2020) 253703.
[48] D.J. Preston, A. Anders, B. Barabadi, E. Tio, Y. Zhu, D.A. Dai, E.N. Wang, Electrowetting-on-dielectric actuation of a vertical translation and angular manipulation stage, Appl. Phys. Lett. 109 (24) (2016) 244102.

Iman Frozanpoor received his MEng degree in Mechanical Engineering (First Class) in 2016 from Northumbria University, UK. He is currently an industrial PhD research student at Durham University, UK. His research topic is the application of electric field induced droplet motion for cleaning platforms in the automotive sector. His main research interests include micro-nano fabrication and microfluidics.

Claudio Balocco MIEEE (Associate professor in Electronic Engineering) received his MSc degree in Electronic Engineering in 2002 and PhD in semiconductor nanodevices in 2006. He has an extensive track record in the development of large-area micro-fabrication and nanofabrication techniques. His area of expertise is further extended to microfluidics and recently have been working on droplet actuation techniques. Dr Balocco research is supported by both UK and European funding bodies as well as through extensive collaboration with industry.

Vibin Ambukan gained his BE (Production Engineering) from India and followed up with MSc (Manufacturing Systems) and PhD (Materials Engineering) at the University of Nottingham, UK. He joined Jaguar Land Rover Research in 2016, where he has been involved in vehicle exterior innovation projects involving active aerodynamics, glazing, autonomous vehicle sensors. In addition, his interests lie in technology transfer and industry-academia collaborative R&D.

Andrew Gallant is a Professor in the Department of Engineering at Durham University. He received his PhD from Durham University in 2004. After this, he worked as a Research Associate in the Microsystems Technology Group at Durham until July 2008 when he was appointed as a Lecturer in 2014, and promoted to a Professor in 2020. His research is focused on the development of micro- and nano-fabricated structures and devices.

Michael Cooke obtained his 1st Class MPhys (Dual-Hons) and PhD from the University of Sheffield. He was also winner of the Hicks Prize for experimental physics. He then joined Durham University to work on initially a nano-magnetic logic project, followed by a second project developing a MEMS probe card. Subsequently, he took a senior experimental role working for ICI on high throughput and microfabricated technologies. This was followed by a 5 year role leading scale-up development at the High Value Manufacturing centre working on organic / plastic electronics. More recently, Dr Cooke returned to Durham University to help develop and manage their microfabrication laboratories.

Diana Ruiz studied for an MPhil in Electrical engineering at the Centre for Research and Advanced Studies in Mexico City before going on to complete a PhD in thermoelectric ceramics at the University of Manchester. After finishing her PhD, she worked as a research associate in the School of Materials at the University of Manchester as part of the MAnufacture of Safe and Sustainable Volatile Element functional materials (MASSIVE) project. She then joined Durham University as an Experimental Officer in Electron Microscopy.